crystals

MDPI

Article

Green Synthesis of Zinc Oxide Nanocrystals Utilizing *Origanum majorana* Leaf Extract and Their Synergistic Patterns with Colistin against Multidrug-Resistant Bacterial Strains

Mohamed Taha Yassin *, Abdulaziz Abdulrahman Al-Askar, Khalid Maniah and Fatimah O. Al-Otibi

Botany and Microbiology Department, College of Science, King Saud University, Riyadh 11451, Saudi Arabia
* Correspondence: myassin2.c@ksu.edu.sa

Abstract: There is a crucial necessity for the formulation of efficient antimicrobial agents owing to the increasing prevalence of hospital-acquired bacterial infections triggered by multidrug-resistant microbes that result in significant deaths and illnesses around the world. Hence, the current investigation examined the antibacterial proficiency of zinc oxide nanoparticles formulated utilizing the green route against bacterial strains that were resistant to multiple drugs. In addition, the synergistic antibacterial action of ZnO nanoparticles (ZnO NPs) combined with colistin was investigated against the tested microbial strains to determine the efficiency of the bioinspired ZnO nanoparticles in boosting the antibacterial proficiency of colistin antibiotic. Incidentally, the bioinspired ZnO nanoparticles were synthesized using water extract of *Origanum majorana* leaves and these nanomaterials were physicochemically characterized using different analytical techniques. The bioactivity of the synthesized nanomaterials against multidrug-resistant bacterial strains was appraised using the agar diffusion method. The biogenic ZnO NPs at a concentration of 100 µg/disk revealed a compelling antimicrobial efficacy against the tested strains, expressing the maximum antimicrobial action against *Escherichia coli* strain with clear zone diameter of 38.16 ± 0.18 mm. The remarkable antibacterial proficiency might be accredited to the tiny particle size of the bioformulated ZnO NPs of 12.467 ± 1.36 nm. The net charge of ZnO nanomaterials was −14.8 mV while XRD analysis confirmed their hexagonal wurtzite structure. Furthermore, the bioformulated ZnO NPs showed a promising synergistic potency with colistin demonstrating respective synergism proportions of 91.05, 79.07, 75.04, 75.25, 56.28 and 10.60% against *E. coli*, *Klebsiella pneumoniae*, *Acinetobacter baumannii*, *Salmonella typhimurium*, *Enterobacter cloacae*, and *Pseudomonas aeruginosa*, respectively. In conclusion, the water extract of *O. majorana* leaves mediated green formulation of zinc oxide nanoparticles with unique physicochemical characteristics and effective antibacterial proficiency against the examined drug-resistant bacterial strains. These nanomaterials could be used in the synthesis of effective antibacterial coatings to control hospital acquired infections caused by multidrug-resistant bacterial pathogens.

Keywords: green synthesis; resistance; zinc oxide nanoparticles; characterization; *Origanum majorana*; synergism; colistin

Citation: Yassin, M.T.; Al-Askar, A.A.; Maniah, K.; Al-Otibi, F.O. Green Synthesis of Zinc Oxide Nanocrystals Utilizing *Origanum majorana* Leaf Extract and Their Synergistic Patterns with Colistin against Multidrug-Resistant Bacterial Strains. *Crystals* **2022**, *12*, 1513. https://doi.org/10.3390/cryst12111513

Academic Editor: Witold Łojkowski

Received: 26 September 2022
Accepted: 21 October 2022
Published: 25 October 2022

1. Introduction

The high prevalence of bacterial microbes that are resistant to different antibiotics is very worrying because multidrug-resistant bacterial pathogens cause a lot of illnesses and deaths around the world [1]. The World Health Organization (WHO) reported a list of pathogens for which new antibiotic development is urgently required in February 2017 to focus and direct research linked to new antibiotics development [2,3]. This list included ESKAPE pathogens, namely, *Enterococcus faecium*, *Staphylococcus aureus*, *Klebsiella pneumoniae*, *Acinetobacter baumannii*, *P. aeruginosa*, and *Enterobacter* species [4]. Recent studies have shown that multidrug-resistant bacterial pathogens as *P. aeruginosa* and *Acinetobacter baumanni* are responsible for roughly 60% of hospital acquired infections [5]. *A. baumannii* is an

opportunistic, gram-negative, and multidrug-resistant bacterial pathogen, responsible for significant number of hospital-acquired infections worldwide [6]. About 45% of all *A. baumannii* isolates in the world were found to be multidrug-resistant pathogens [7]. Alarmingly, *P. aeruginosa* is an opportunistic bacterial pathogen causing severe respiratory infections in people with impaired immune systems [8]. Furthermore, *P. aeruginosa* accounts for about 10% of the nosocomial infections worldwide [9]. Additionally, *Klebsiella pneumoniae* is a nosocomial multidrug-resistant pathogen accounting for significant number of morbidities and mortalities worldwide, owing to the limited treatment options [10]. *K. pneumoniae* has found to be a significant source of hospitalized infections, particularly among patients in intensive-care units of neonates, recording mortality rates can be as high as 70% [11]. In the past ten years, *Enterobacter cloacae* has been one of the *Enterobacter* spp. most frequently responsible for nosocomial infections [12]. Due to the production of β-lactamase enzymes, *E. cloacae* has an inherent resistance to amoxicillin, ampicillin, cefoxitin and first-generation cephalosporins [13]. On the other hand, *E. coli* is recognized as a crucial etiological agent of urinary tract infections (UTI) and bloodstream infections in both healthcare and community settings globally [14]. In this regard, *E. coli* is the most frequent gram-negative bacterial pathogen isolated from urine and blood cultures in Australian emergency and inpatient department settings [15]. *Salmonella typhimurium* is a facultative, anaerobic, gram-negative bacterial strain causing foodborne illness known as salmonellosis [16]. The bacterial resistance of *S. Typhimurium* to cephalosporins or ciprofloxacin antibiotics has reportedly evolved in countries such as the United States and France [17].

Nanotechnology is an emerging, fast growing and interesting field of science and technology due to its large number of potential biomedical applications [18]. Nanoparticles have a large surface area to volume ratio and a small size range of 1 to 100 nm, which makes them beneficial for a multiplicity of substantial biomedical applications [19]. Recently, metal oxide nanoparticles have drawn a lot of interest due to their unique physicochemical characteristics that could be applied in a range of biomedical applications [20]. There are different ways to synthesize nanoparticles, including physical, chemical, and biological approaches [21]. Due to the economical and the environmental concerns, the green way of synthesizing nanoparticles is a good substitute to the chemical and physical processes [22]. Physical and chemical methods that have been used for a long time to formulate nanoparticles take less time, but they need toxic chemicals acting as protective agents to keep them stable, resulting in increased toxicity in the environment [23]. With this in mind, green nanotechnology that uses plants is becoming more popular as an ecofriendly, safe, cheap, and non-toxic option [24]. The plant extract-mediated biosynthesis of nanoparticles utilizes proteins as natural capping agents [25]. In addition, utilizing plant extracts in the bioformulation of metal oxide nanoparticles is safer, simpler, faster, cheaper, and more ecofriendly than using microbial assistance [26]. The plant parts as roots, stems, fruits, leaves and seeds were reported to be rich in the phytochemical components such as polyphenolic compounds, polysaccharides, alkaloids, vitamins, amino acids, and terpenoids which can reduce the metal ions or metal oxides to 0 valence metal nanoparticles [27]. Furthermore, the plant metabolites are crucial for the capping, stabilization, and reduction of the biosynthesized nanoparticles [28]. In more detail, the phytochemicals in plant extract bioreduce Zn ions to synthesize nanoparticles, which later interact with dissolved oxygen to formulate ZnO NPs [29]. It is well recognized that zinc oxide nanoparticles have important biological and therapeutic uses. ZnO NPs are classified as safe according to the US Food and Drug Administration's recommendations (i.e., generally recognized as safe) [30].

Zinc oxide nanoparticles among nanosized metal oxides have been signified to retain a potential anticarcinogenic, and antibacterial properties in consequence of their distinctive physicochemical characteristics [31]. A recent report indicated that *Phoenix roebelenii* leaves intermediated green formulation of ZnO NPs which were established to display antimicrobial effectiveness against gram-positive (*Streptococcus pneumoniae* and *S. aureus*) and gram-negative (*S. typhi* and *E. coli*) bacterial strains [32]. Another investigation revealed

the sustainable bioformulation of ZnO NPs utilizing *Cucumis melo* extract, showing the maximum antimicrobial proficiency against *E. coli* strain recording inhibition zone diameter of 9.85 ± 0.68 mm at a concentration of 150 µg/mL [33]. The antimicrobial efficacy of green synthesized ZnO NPs utilizing *Terminalia catappa* leaf extract against *S. aureus* and *E. coli* was reported to be higher than that of chemically synthesized ZnO NPs [34]. The mode of antimicrobial action of ZnO NPs is a four-step process that begins with the high affinity of ZnO NPs for bacterial cells, hydrogen peroxide production from ZnO NPs surface, interaction also with phosphorus and sulfur containing molecules as DNA, and finally arresting the biological metabolism of microbial cells by disrupting their protein molecules, resulting in bacterial cell death [35].

A previous investigation has evaluated the synergistic pattern of ZnO NPs and antibiotics combination and reported the potential antibacterial efficacy of ZnO NPs combination with norfloxacin, ofloxacin, cephalexin antibiotics against *S. aureus*, *E. coli*, and *P. aeruginosa* strains [36]. In addition, another report demonstrated the boosting influence of ZnO NPs on the antibacterial efficiency when combined with ciprofloxacin and imipenem antibiotics [37]. The sweet marjoram plant, *Origanum majorana* L., is a perennial herb in the Lamiaceae family [38]. *Origanum majorana* extracts were reported to possess antimicrobial, antiparasitic, antidiabetic, antioxidant, anticancer, anti-inflammatory and hepatoprotective activities [39].

The synergistic antimicrobial proficiency of chemically synthesized ZnO NPs with colistin antibiotic was assessed against clinical isolates of *P. aeruginosa* and the authors reported that colistin and ZnO NPs could be utilized as potential therapeutic agents for treatment of *P. aeruginosa* illnesses, owing to their potential synergistic action [40]. Another report demonstrated the antimicrobial synergism between colistin and silver nanoparticles at a concentration of 10 µg/disk against different nosocomial bacterial pathogens [41]. In addition, silver oxide nanoparticles (Ag_2O NPs) showed synergistic activity with colistin against multidrug-resistant bacterial pathogens causing wound infections and also proved to be biocompatible with human dermal fibroblasts [42]. Previous studies looked at the synergistic effects of green-formulated silver and silver oxide nanoparticles, as well as chemically-formulated ZnO NPs, against different drug-resistant bacterial strains. However, none of these studies used green-formulated ZnO NPs synthesized from plant extracts against a wide range of nosocomial bacterial pathogens, which is why this study was conducted to determine if colistin and ZnO NPs could work together in a synergistic manner.

Finding new antibacterial agents is urgently needed due to the high prevalence of bacterial resistance, so the aqueous extract of *O. majorana* was utilized to formulate green ZnO NPs, and their bioactivity against drug-resistant strains was assessed. In addition, few studies have assessed the synergistic antimicrobial effectiveness of ZnO NPs with colistin. Hence, the current investigation evaluated the synergistic pattern of ZnO NPs synthesized using *O. majorana* water extract with colistin antibiotic against seven bacterial strains, which were found recently to exhibit high resistance patterns.

2. Materials and Methods

2.1. Preparation of Aqueous Extract of O. majorana Leaves

The *Origanum majorana* leaves were acquired from local markets in Riyadh, Saudi Arabia. Identification of the plant material was accomplished by the Herbarium of Botany and Microbiology Department. The gathered leaves were first washed twice with tap water and once with sterile distilled water. A mechanical blinder was utilized to macerate the dried leaves, and 50 g of the homogenized powder was then dissolved in 500 mL flasks encompassing 200 mL of sterile deionized water. The flasks were then heated at 50 °C for 30 min over a hot plate. Finally, the flasks were stirred over a magnetic stirrer for 24 h at 25 °C and then filtered using Whatman filter paper grade 1 to attain clear filtrates. The extracts were refrigerated at 4 °C for subsequent usage [43–47].

2.2. Green Formulation of ZnO NPs

The biosynthesis of ZnO NPs utilizing *O. majorana* extract was achieved utilizing 0.01 M zinc nitrate hexahydrate (Zn $(NO_3)_2 \cdot 6H_2O$) solution. Zinc nitrate hexahydrate (Zn $(NO_3)_2 \cdot 6H_2O$) of reagent grade 98% was obtained from Sigma-Aldrich, U.K. In essence, 5 mL of water extract from *O. majorana* leaves was combined with 95 mL of zinc nitrate solution (0.01 M), and the combination was stirred with a magnetic stirrer for an hour at 70 °C (150 rpm). The bioformulation of ZnO NPs was detected by formation of reduced precipitates. Finally, the bioreduced precipitates of ZnO NPs were harvested by centrifugation for 10 min at 10,000 rpm. After discarding the supernatants, the collected precipitates were washed three times with sterile distilled water for the elimination of the impurities [48].

2.3. Characterization of the Bioformulated ZnO NPs

The dried ZnO NPs were characterized via the methods previously described in a prior study, including UV-Vis Spectroscopy, Energy Dispersive X-ray (EDX) analysis, Transmission Electron Microscopy (TEM) analysis, FTIR (Fourier-transform infrared) analysis, X-ray powder diffraction (XRD), and zeta potential analysis. Briefly, UV-Vis Spectroscopy was utilized to estimate the optical spectrum in wavelengths ranged from 200 to 800 nm and the elemental configuration of ZnO NPs was achieved using energy-dispersive X-ray (EDX) analysis. However, ZnO NPs shape and size were detected using the TEM technique. In this regard, the biofabricated ZnO nanoparticles were washed three times in a row with deionized water to prepare them for TEM analysis. Afterwards, the samples were then laid over a carbon-coated copper grid, peeled off, and allowed to dry before being examined. TEM analysis was conducted using a Transmission Electron Microscope (JEOL, JEM1011, Tokyo, Japan), which generated high-resolution two-dimensional images at 100 kv voltage for the detection of the size, morphology and particle size distribution. The crystalline properties of the formulated nanomaterials were detected using XRD analysis, while the net charge and the hydrodynamic particle size of ZnO nanomaterials were detected using zeta potential analysis [49]. X-ray powder diffraction (XRD) examination was carried out using a Shimadzu XRD model 6000 diffractometer (Shi-madzu, Columbia, IN, USA) equipped with a graphite monochromator that generated Cu-K radiation to yield XRD patterns.

2.4. Screening of the Antimicrobial Proficiency of the Bioformulated ZnO NPs

The antimicrobial proficiency of the bioformulated ZnO NPs was appraised using the agar diffusion technique [50]. The American Type Culture Collection provided the bacterial strains used in the study, which included the following strains: *A. baumannii* (ATCC 43498), *E. cloacae* (ATCC 13047), *E. coli* (ATCC 25922), *K. pneumoniae* (ATCC 700603), *S. typhimurium* (ATCC 14023), and *P. aeruginosa* (ATCC 9027). For bacterial suspension preparation, sterile loops were utilized to harvest the bacterial colonies from freshly prepared bacterial cultures, which were subsequently dispersed in 0.9% normal Saline. The bacterial suspension turbidity was adjusted using 0.5 McFarland standard to attain viable bacterial cell count of 10^8 cfu/mL. Sterile Mueller Hinton agar (MHA) plates were prepared, then 0.5 mL of the processed bacterial suspension was distributed homogenously over the surface of the plates. The dried ZnO NPs were first dissolved in methanol and then sonicated to guarantee the complete solubility of these nanomaterials. Sterilized disks of filter paper (8 mm in diameter) were then filled with 50 and 100 µg of the dissolved ZnO NPs. Colistin sulfate (CAS No.1 264-72-8, purity ≥99.9%) was supplied from Sigma-Aldrich (St. Louis, MO, USA). Filter paper disks loaded with just methanol solvent were used as negative controls, whereas colistin disks (10 µg) were utilized as positive controls. Consequently, ZnO disks and both of negative and positive control disks were positioned over the inoculated MHA plates. The plates were preserved for 24 h at 37 °C in incubator after being refrigerated for 2 h to enable ZnO NPs diffusion. Finally, the suppressive zone diameters were estimated using Vernier caliper. For the detection of minimum inhibitory concentration (MIC), broth microdilution assay was achieved using 96-well microtiter plates against the *E. coli* strain which demonstrated the highest sensitivity to the bioformulated ZnO nanomaterials [51].

In addition, inoculums from MIC wells were streaked over newly poured MHA plates to estimate the minimum bactericidal concentration (MBC) and the inoculated plates were then preserved at 37 °C for 24 h in an incubator. MBC was recognized as the lowermost concentration of the bioformulated ZnO NPs expressing no microbial growth [52].

2.5. Detection of the Synergistic Patterns of the Bioformulated ZnO NPs with Colistin

The ability of the bioformulated ZnO NPs to improve the antimicrobial potency of colistin antibiotic was assessed using the standard disk diffusion assay [53,54]. A group of 8 mm disks was filled with the MIC concentration of the biogenic ZnO NPs (15 µg/disk). One batch of filter paper disks was impregnated with ZnO NPs (15 µg/disk) and colistin (10 µg/disk) whereas another group was loaded with just the antibiotic colistin (10 µg/disk). Negative control disks were solely filled with the methanol solvent. Inoculated MHA plates were adjusted as previously described then the filled filter paper disks were positioned over the surface of the inoculated plates. Incubation of the plates at 37 °C for 24 h was achieved after refrigeration of these plates for 2 h at 4 °C to permit ZnO NPs nanoparticles. Vernier caliper was utilized to measure the inhibitory zone diameters, and the following equation was used to determine the synergistic effectiveness of bioformulated ZnO NPs: synergism % = $\frac{B-A}{A} \times 100$, whereas A is the colistin suppressive zone diameter and B is the inhibitory zone diameter of both of ZnO NPs + colistin [55].

2.6. Statistical Analysis

GraphPad Prism 8.0 (GraphPad Software, Inc., La Jolla, CA, USA) was utilized to investigate the representative data, and the results were tabulated as mean of triplicates ± standard error. One-way analysis of variance and Tukey's test were used to evaluate these data in order to find significant differences between the estimated values.

3. Results and Discussion

3.1. Green Bioformulation of ZnO NPs

The bioformulation of biogenic ZnO NPs was conducted using water extract of sweet marjoram as presented in Figure 1. In this regard, the biosynthesis of ZnO NPs was initially confirmed through the formation of the reddish-brown precipitate after the addition of *O. majorana* extract to the colorless zinc nitrate solution, as seen in Figure 2. The formation of reddish-brown precipitate was formerly described as a preliminary indication for the biofabrication of ZnO NPs [56,57]. Plant extracts are known to be rich in phytochemical constituents as phenolic acids, flavonoids, methylxanthines and saponins [58]. These constituents are known as antioxidants owing to their capability to neutralize free radicals, reactive oxygen species (ROS), and chelate metals [59]. Aqueous extract of *O. majorana* is reported to possess a high content of antioxidants contributing to its potent antiproliferative and antioxidant activities [60]. Accordingly, it is assumed that the phytoconstituents found in *O. majorana* leaves as phenolic compounds, flavonoids, amides, alkenes and proteins are accountable for the biofabrication of ZnO NPs due to their ability to reduce or chelate metal ions and to act as stabilizing and capping agents for the biogenic ZnO NPs [61–63]. Another report demonstrated that phytochemical components designated their electrons and granted to the biostabilization of Zn^{2+} ions; thereafter, Zn^{2+} complex ions were converted to ZnO NPs via thermal annealing [64].

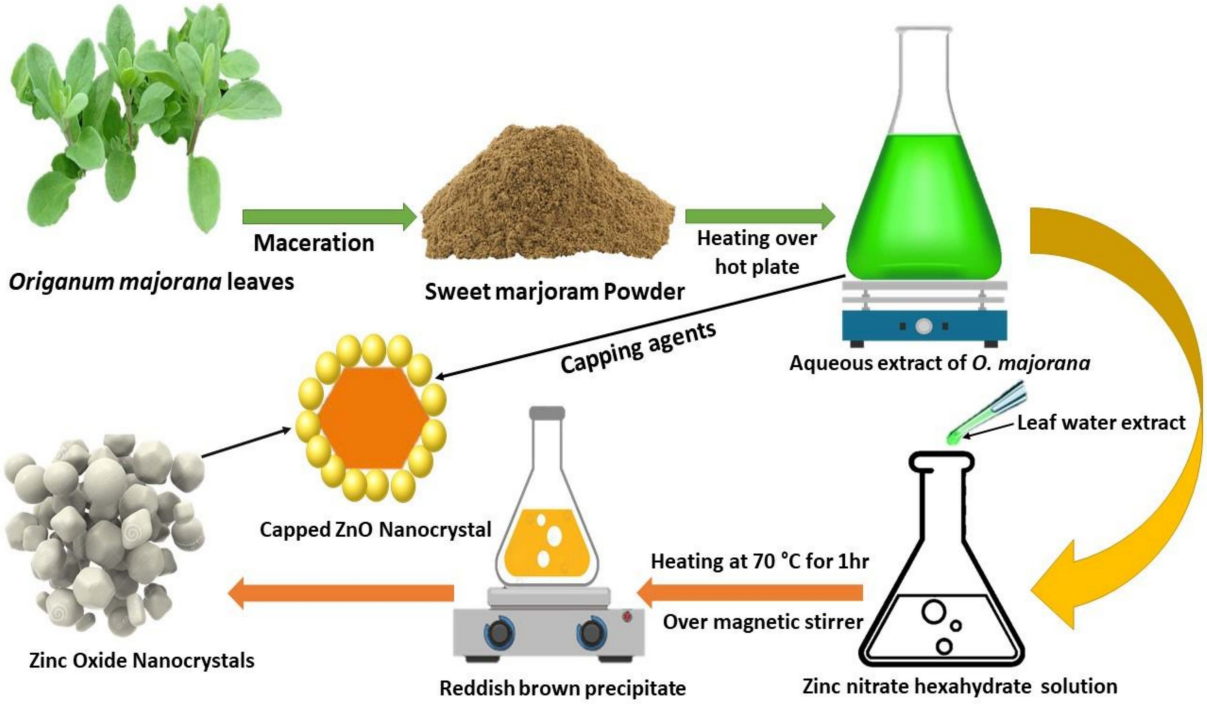

Figure 1. Schematic illustration describing the workflow of ZnO NPs synthesis.

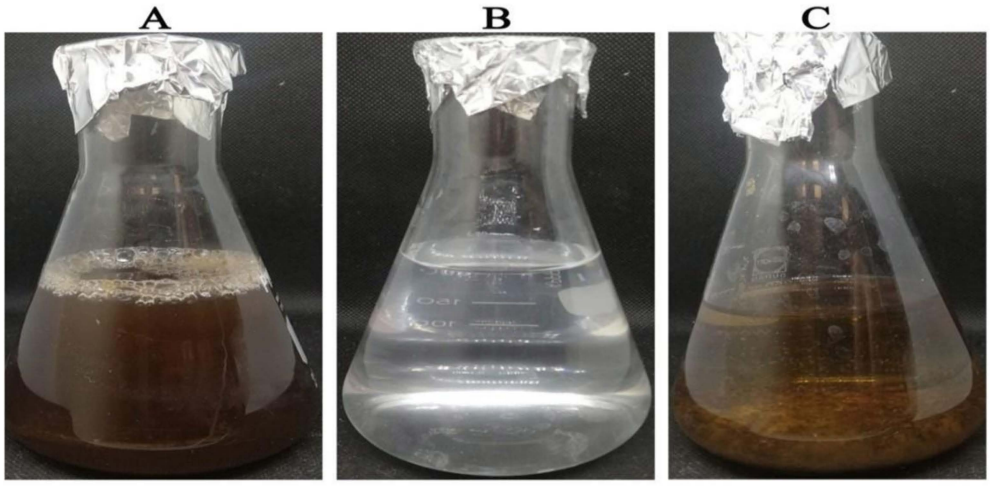

Figure 2. Green bioformulation of ZnO NPs using water leaf extract of sweet marjoram. (**A**) *O. majorana* aqueous extract; (**B**) colorless solution of zinc nitrate hexahydrate; (**C**): formation of reddish-brown precipitate, indicating synthesis of ZnO NPs.

3.2. UV Spectral Analysis

UV spectral analysis of ZnO NPs formulated utilizing *O. majorana* extract showed the detection of three absorption peaks at 242, 395 and 420 nm (Figure 3). The sharp emission peaks at 395 and 420 nm could be allocated to the surface plasmon resonance of the biosynthesized ZnO NPs while the emission peak at 242 nm could be assigned to the *O. majorana* extract as reported in previous reports [62,65]. The Tauc plot method was used to estimate the band gap energy of the biosynthesized ZnO nanomaterials [66]. The estimated band gap energy of the biogenic ZnO NPs was 3.10 eV, as shown in Figure 4. Our results were in accordance with that of Fatimah et al., 2016, who revealed that the band gap energy of ZnO NPs formulated using ethanolic leaf extract of *Mimosa Pudica* was 3.10 eV [67].

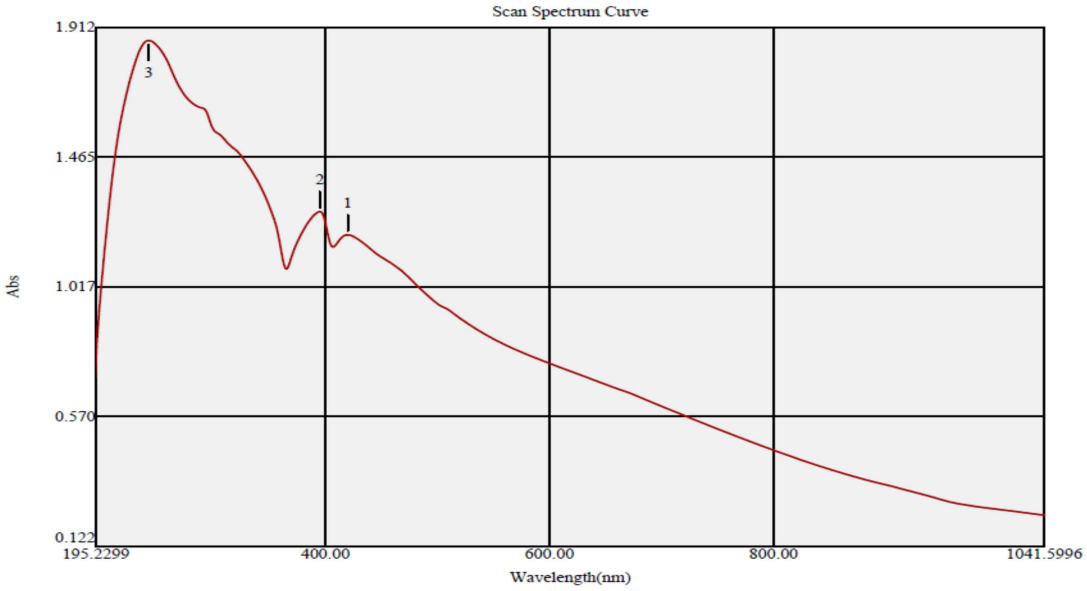

Figure 3. UV spectrum of the biogenic ZnO NPs synthesized using *O. majorana* extract (peak no 1: 420 nm, peak no 2: 395 nm, peak no 3: 242 nm).

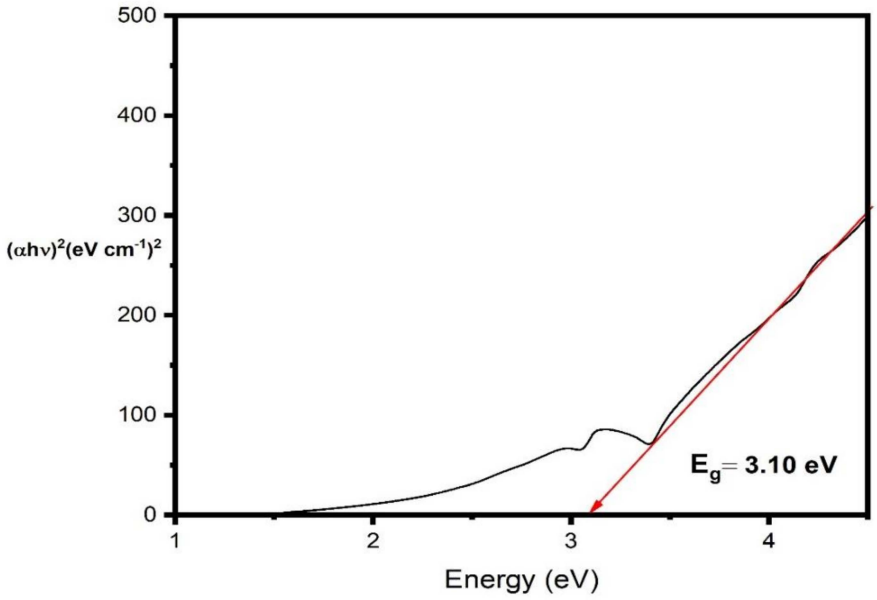

Figure 4. Band gap energy of the biogenic ZnO NPs using the Tauc plot method.

3.3. Transmission Electron Microscope (TEM) Analysis

The size and morphology of the bioformulated ZnO NPs were investigated using TEM analysis [68]. The biogenic ZnO NPs were depicted in Figure 5 in a multiplicity of shapes, including hexagons, spheres, and quasi-spheres. Additionally, the size distribution histogram demonstrated that the biogenic ZnO NPs had an estimated average nanosize of 12.467 nm and fluctuated in size from 5 to 50 nm in diameter (Figure 6). An earlier work reported that the particle size diameters of ZnO NPs synthesized using fresh and dry alhagi plant extract were 40 and 70 nm, respectively. The estimated nanosize of the bioformulated ZnO NPs (12.467 nm) was less than those revealed in that study [69]. Our results were in agreement with that of a prior report which demonstrated that *Sageretia thea* (Osbeck) facilitated green bioformulation of ZnO NPs with a typical particle size diameter of 12.4 nm [70]. The small nanosized ZnO NPs affirmed the high effectiveness of the green route of ZnO NPs synthesis using water leaf extract of *O. majorana*.

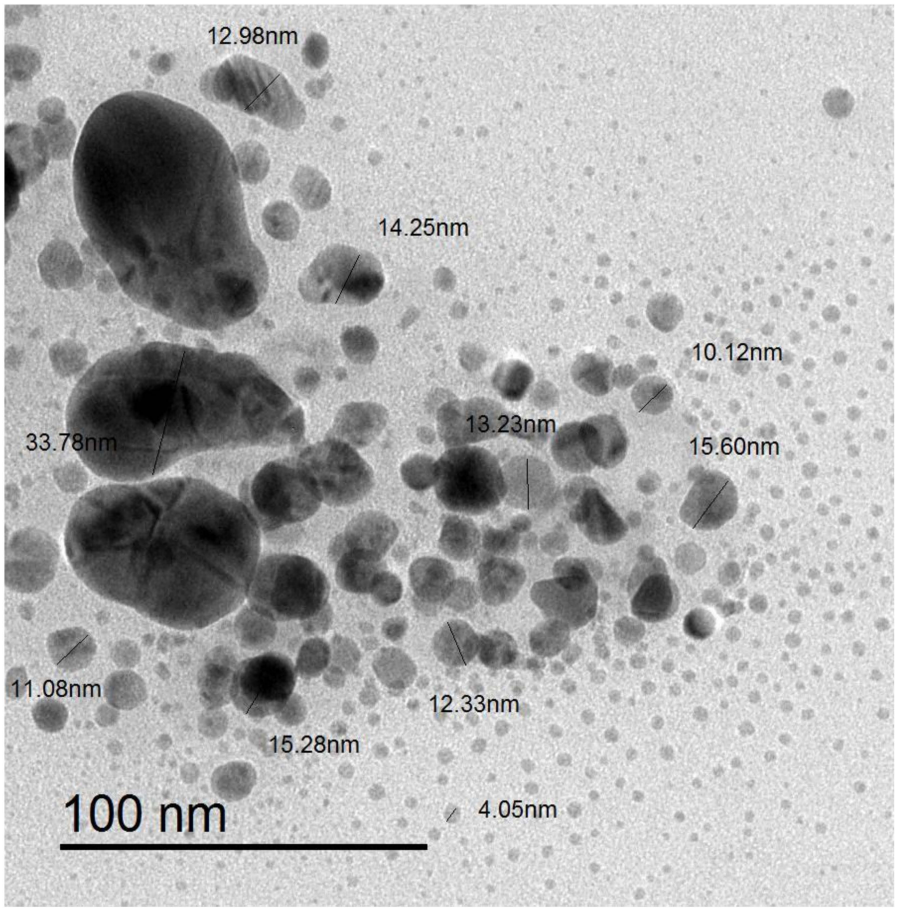

Figure 5. TEM micrograph of ZnO NPs synthesized using *O. majorana* extract.

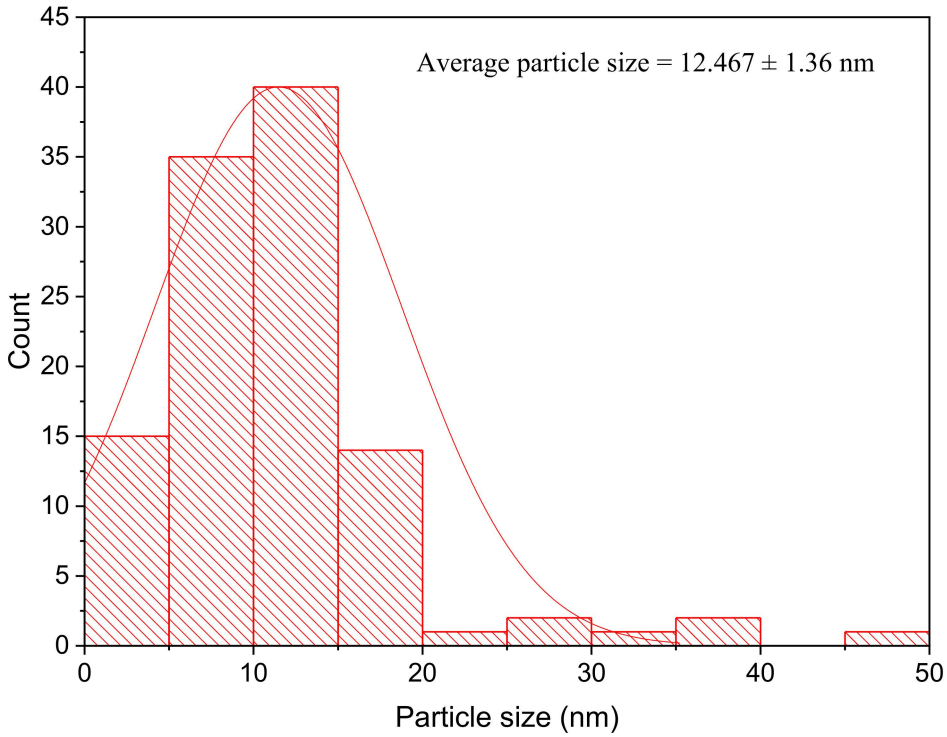

Figure 6. Size distribution pattern of ZnO NPs formulated utilizing *O. majorana* extract.

3.4. Energy-Dispersive X-ray (EDX) Analysis

The elemental configuration of the biogenic ZnO NPs was achieved utilizing EDX analysis. The EDX spectrum revealed the presence of zinc and oxygen elements recording relative percentages of 23.38 and 34.38%, respectively, affirming the successful formulation of ZnO NPs (Figure 7). Contrastingly, the other peaks as C, Ca, P, and Al could be assigned to the breakdown of capping agents of the *O. majorana* extract, such as amino acids, sugars, proteins and polysaccharides owing to X-ray emissions [71]. Furthermore, the observed peak of carbon element could be attributed to the carbon tape which was used for sample preparation [72]. The Zn peaks detected at 1.1, 8.6 and 9.5 keV could be accredited to Zn Lα, Zn Kα and Zn Kβ, respectively [73].

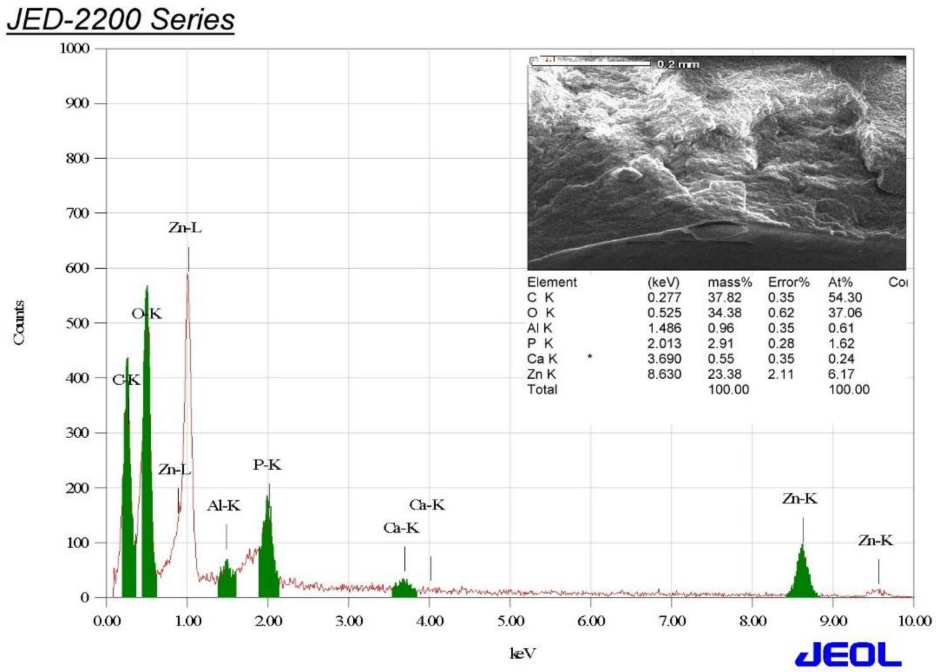

Figure 7. EDX spectrum of the biosynthesized ZnO NPs.

3.5. Fourier-Transform Infrared Spectroscopy (FTIR) Analysis

The main functional groups contributing to the reduction, stabilization and capping of the bioformulated ZnO NPs were detected using FTIR analysis [74]. The FTIR spectrum revealed different absorption peaks at 3430.50, 1628.74, 1509.02, 1396.52, 1263.40, 1048.02 and 580.03 cm^{-1} (Figure 8). The strong peak detected at 3430.50 cm^{-1} could be ascribed to the hydroxyl functional groups which correlated to the polyphenolic constituents of the plant extract contributing to the reduction and biostabilization of ZnO NPs [75]. Another investigation demonstrated that the wide absorption peak noticed at 3430 cm^{-1} could be allotted to the O-H stretching vibrations of phenolic constituents of *Azadirachta Indica* leaf extract contributing to the stabilization and capping of ZnO NPs [76]. The other absorption peaks observed at 1628.74 cm^{-1} and 1509.02 cm^{-1} were reported to be due to the molecular vibrations of double-bonded carbon stretching (Table 1). [77,78]. Moreover, the small band detected at 1396.52 cm^{-1} could be recognized to the C=O stretching of carboxylic acids [79]. However, a tiny band at 1263.40 cm^{-1} in the spectra was attributed to the C-N stretching of amines, which were described to serve as capping agents on ZnO NPs surface [80]. The band detected at 1048.02 cm^{-1} was informed to be owing to C−C stretching of alcohols which might be capped over ZnO NPs surface [81]. However, the broad absorption band at 580.03 cm^{-1} was reported to be characteristic for metal oxide bond (Zn–O), indicating the bioformulation of ZnO NPs [82]. Collectively, the detected functional groups of biogenic ZnO NPs such as phenols, alcohols, amines, alkenes and

carboxylic acids contributed significantly to the reduction, stabilization and capping of the biofabricated nanomaterials [83].

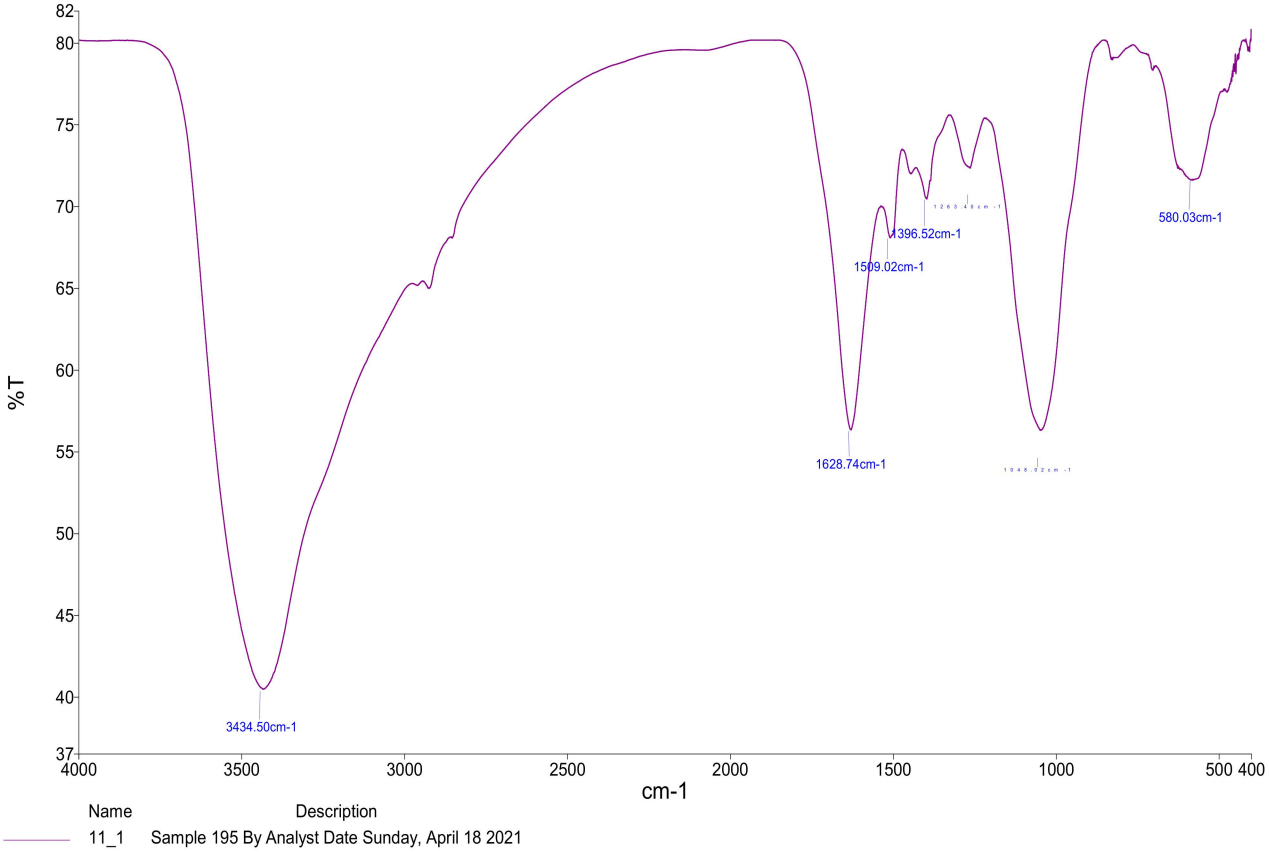

Figure 8. FTIR spectrum of ZnO NPs formulated using *O. majorana* extract.

Table 1. Functional groups of the biosynthesized ZnO NPs formulated using *O. majorana* extract.

No.	Absorption Peak (cm^{-1})	Appearance	Functional Groups	Molecular Motion
1	3434.50	Strong, broad	Phenols	O-H stretching
2	1628.74	Medium	Cyclic alkene	C=C stretching
3	1509.02	Weak	Alkenes	C=C stretching
4	1396.52	Weak	Carboxylic acids	C=O stretching
5	1263.40	Weak	Amines	C–N stretching
6	1048.02	Medium	Alcohols	C−C stretching
7	580.03	Medium	Metal oxide bonds	Zn-O stretching

3.6. X-ray Diffraction (XRD) Analysis of the Biofabricated ZnO NPs

The crystallographic nature of the bioformulated ZnO NPs was investigated utilizing XRD analysis. Additionally, the XRD configuration demonstrated the detection of seven diffraction peaks at 2θdegrees of 31.56, 34.32, 36.69, 46.63, 57.05, 64.79 and 77.73° as shown in Figure 9, conforming to the planes of (100), (002), (101), (102), (110), (103), and (104), respectively [84]. These results were in agreement with those documented in the Joint Committee on Powder Diffraction Standards (JCPDS, card No. 89-7102). Collectively, these results established the hexagonal wurtzite configuration of the bioformulated ZnO NPs [85]. Our results were consistent with a prior report that described the eco-friendly bioformulation of ZnO NPs utilizing *Plectranthus amboinicus* leaf extract, confirming the formation of hexagonal wurtzite structure as demonstrated by XRD data that shown the detection of diffraction peaks at 2θdegrees of 31, 34, 36, 47, 56, 62, 66, 67, and 68°,

conforming to the crystal planes (100), (002), (101), (102), (110), (103), (200), (112) and (201), respectively [86]. The crystalline size of the biogenic ZnO nanoparticles was estimated according to Scherrer's formula as follows: $D = (k\lambda/\beta \cos \theta)$, where D is the nanosize of the biogenic ZnO nanoparticles, λ is wavelength of X-ray (1.54178 Å), K is Scherer's constant (K = 0.94), β is full width at half maximum (FWHM) of the most intense diffraction peak, which is detected to be 0.6912, and θ is the diffraction angle (36.69°) [87]. In this regard, the crystalline size was calculated using the peak with the highest intensity, which corresponds to the plane (101) at 36.69°, and it was found to be 12.65 nm. This result was consistent with the results of the TEM analysis.

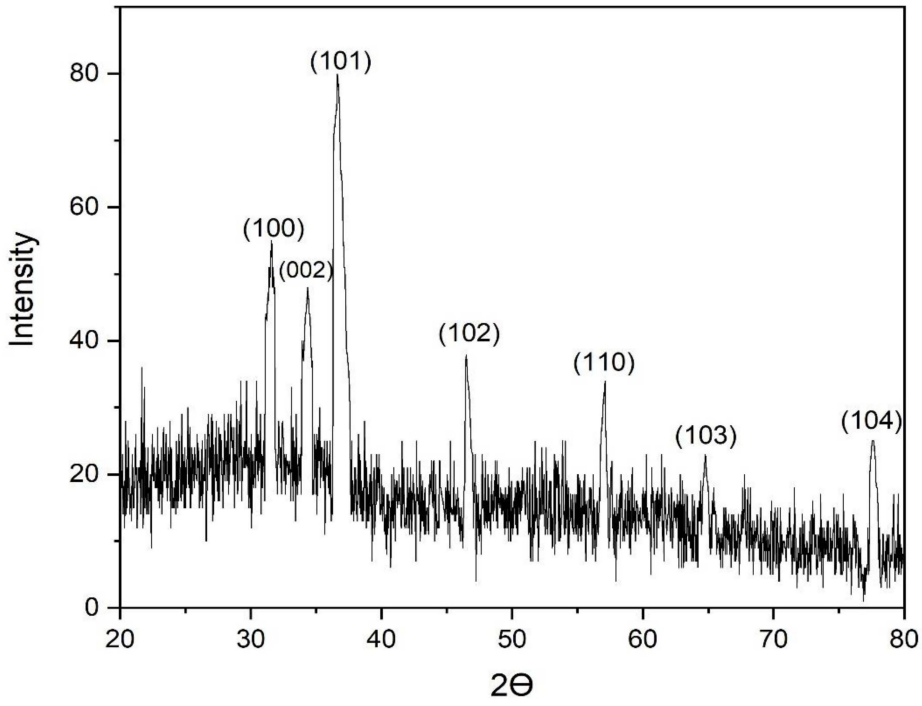

Figure 9. XRD spectrum of the biosynthesized zinc oxide nanoparticles utilizing *O. majorana* extract.

3.7. Zeta Analysis of ZnO NPs

Using a Zetasizer Nano ZS, the dynamic fluctuations in light scattering intensity (DLS) were used to estimate the size distribution pattern of the biogenic ZnO NPs [88]. That measurement provided the crest values of the hydrodynamic diameter distribution pattern, the polydispersity index (PdI), which indicated the width of the particle size distribution, and the average hydrodynamic diameter of the biogenic ZnO NPs [89]. The PdI scale runs from 0 to 1, with 0 representing monodisperse and 1 representing polydisperse materials [90].

The dynamic light scattering (DLS) technique revealed a polydispersity index of 0.453 with an average hydrodynamic size of 71.93 nm (Figure 10). The estimated hydrodynamic size was higher than that of TEM, due to the capping and stabilizing action of phytoconstituents on the surface of ZnO NPs [91]. Additionally, the large measured hydrodynamic size in comparison to the size detected by TEM micrographs could be assigned to the deposition of additional hydrate layers over the surface of zinc oxide nanocrystals [92]. Our results were in accordance with a prior study that showed the average hydrodynamic diameter of ZnO NPs to be 70 nm while the average particle diameter according to TEM measurements was 37.5 nm. The authors attributed this to the aggregation of nanoparticles [93]. Additionally, the surface charge of the biogenic zinc oxide nanoparticles was estimated using zeta potential analysis and was found to be −14.8 mV (Figure 11). Our results were consistent with those of a previous report which demonstrated the green formulation of ZnO NPs utilizing leaf extract of *Rhamnus virgata*, recording a net surface

charge of −13 mV [94]. The size distribution of the biosynthesized ZnO NPs was represented by the PDI [95]. Practically, the PDI value indicated the potential effectiveness of the bioformulated ZnO NPs for biological applications and should be less than 0.5 [96]. Interestingly, the detected PDI value of the biogenic ZnO NPs was 0.453. Collectively, the biosynthesized ZnO nanomaterials revealed unique physicochemical characteristics, enabling the potential use of these nanomaterials in biomedical applications.

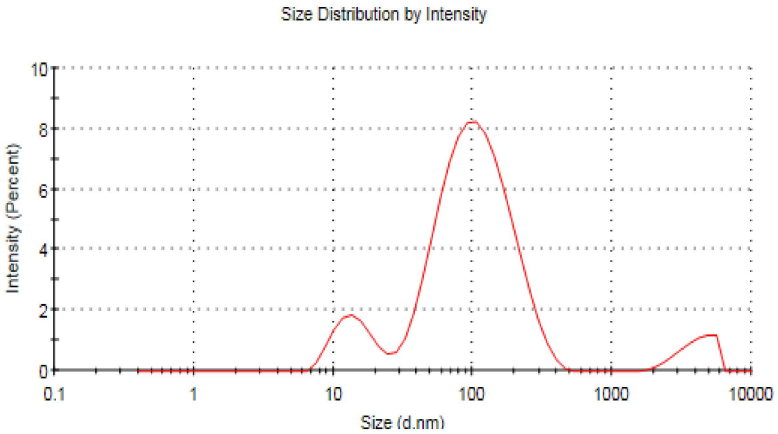

Figure 10. Dynamic light scattering of the biogenic ZnO NPs.

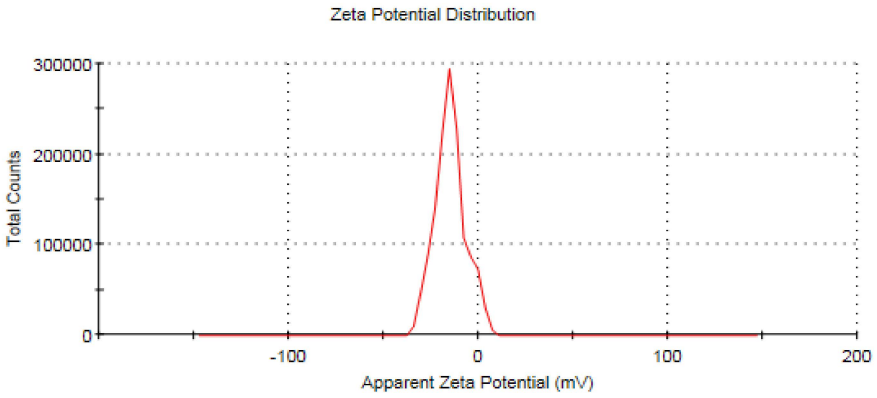

Figure 11. Zeta potential analysis of the biofabricated ZnO NPs.

3.8. Screening of the Antimicrobial Efficiency of the Biosynthesized ZnO NPs

The antimicrobial patterns of the bioformulated ZnO were screened against the concerned bacterial strains using the standard disk diffusion assay. In this respect, the *E. coli* strain revealed the maximum sensitivity to different ZnO NPs concentrations of 50 and 100 µg/disk, demonstrating the inhibitory zone diameter of 32.16 and 38.16 mm, respectively (Table 2). On the other hand, *P. aeruginosa* revealed the lowermost sensitivity to ZnO NPs at concentrations of 50 and 100 µg/disk, registering inhibitory zone diameters of 13.18 and 16.24 mm, respectively. The other tested strains as *A. baumannii*, *E. cloacae*, *K. pneumoniae* and *S. typhimurium* strains demonstrated sensitivity to the biogenic ZnO NPs (100 µg/disk), registering inhibition zone diameters of 19.31, 24.12, 26.47 and 22.86 mm, respectively. Our results were in accordance with those of Subramanian et al., 2022, who reported that *Sargassum muticum* extracts facilitated green bioformulation of zinc oxide nanoparticles (80 µg/mL), demonstrating a suppressive zone of 18 mm against *A. baumannii* strain [97]. The mode of antibacterial action of the biogenic zinc oxide nanoparticles uses a biphasic phenomenon that is predisposed by osmotic shock, which breaks microbial cell membranes and internalizes the nanoparticles, resulting in reactive oxygen species (ROS) generation, oxidative stress, and eventually cell death [98].

Table 2. Antimicrobial efficiency of the biosynthesized ZnO NPs against different bacterial pathogens.

The Bacterial Strains	Inhibition Zone Diameter (mm)			
	ZnO NPs (50 µg/Disk)	ZnO NPs (100 µg/Disk)	Colistin (10 µg/Disk)	−ve Control
A. baumannii	17.14 ± 0.27	19.31 ± 0.56	11.13 ± 0.19	0.00 ± 0.00
E. coli	32.16 ± 0.49	38.16 ± 0.18	27.13 ± 0.45	0.00 ± 0.00
E. cloacae	21.65 ± 0.52	24.12 ± 0.23	14.08 ± 0.14	0.00 ± 0.00
K. pneumoniae	23.87 ± 0.16	26.47 ± 0.38	18.98 ± 0.15	0.00 ± 0.00
P. aeruginosa	13.18 ± 0.11	16.42 ± 0.31	15.93 ± 0.29	0.00 ± 0.00
S. typhimurium	20.13 ± 0.24	22.86 ± 0.18	17.15 ± 0.36	0.00 ± 0.00

The potential antimicrobial effect of the bioformulated ZnO NPs could be allotted to the small particle size of the bioformulated nanoparticles which was noticed to be 12.467 nm according to TEM measurements [99]. The small particle size of ZnO NPs has the potential ability to penetrate the microbial cells due to the increased surface area to volume ratio [100]. Accordingly, the small ZnO nanoparticles are more effective antibacterial agents than larger ones [101]. The minimum inhibitory concentration (MIC) of the biofabricated ZnO NPs was investigated against the *E. coli* strain as it showed the highest susceptibility to the formulated ZnO nanomaterials. The MIC of the bioformulated ZnO nanomaterials was noticed to be 15 µg/mL while the minimal bactericidal concentration was detected to be 20 µg/mL.

3.9. Detection of the Synergistic Potency of the Biosynthesized ZnO NPs with Colistin

The biosynthesized ZnO NPs were examined for their synergistic antimicrobial efficacy effectiveness with colistin antibiotic against the relevant bacterial strains, since these pathogens had significant drug-resistance profiles [102]. Table 3 displayed the suppressive zone diameters of both colistin and the biosynthesized ZnO NPs to investigate the synergistic patterns of the biosynthesized ZnO NPs in boosting the antimicrobial action of colistin.

Table 3. Synergistic antimicrobial proficiency of the biofabricated ZnO NPs with colistin against the multidrug-resistant strains.

The Tested Strains	Inhibition Zone Diameter (mm)			
	Colistin (10 µg/Disk)	ZnO NPs (15 µg/Disk)	Colistin (10 µg/Disk) + ZnO NPs (15 µg/Disk)	−ve Control
A. baumannii	11.78 ± 0.23	10.35 ± 0.11	20.62 ± 0.14	0.00 ± 0.00
E. coli	17.89 ± 0.18	16.95 ± 0.38	34.18 ± 0.25	0.00 ± 0.00
E. cloacae	14.16 ± 0.56	15.18 ± 0.49	22.13 ± 0.32	0.00 ± 0.00
K. pneumoniae	15.29 ± 0.09	16.84 ± 0.24	27.38 ± 0.41	0.00 ± 0.00
P. aeruginosa	14.89 ± 0.16	8.98 ± 0.12	16.42 ± 0.46	0.00 ± 0.00
S. typhimurium	13.78 ± 0.51	14.97± 0.43	24.15 ± 0.17	0.00 ± 0.00

The biogenic ZnO NPs revealed the highest synergistic efficiency with colistin against *E. coli* strain while the lowest synergistic activity was detected against *P. aeruginosa* strain recording relative synergistic percentages of 91.05 and 10.60%, respectively (Figure 12). Correspondingly, a previous report indicated that *E. coli* strain was significantly susceptible to ZnO NPs combined with antibiotics as oxacillin, azithromycin, cefuroxime, cefotaxime, oxytetracycline and fosfomycin compared to antibiotics alone. In addition, the synergistic

action of ZnO NPs with different antibiotics as oxacillin, azithromycin, cefotaxime, fosfomycin, cefuroxime, and oxytetracycline against *E. coli* was described to be significantly higher in comparison with antibiotic alone [103]. Our findings were also in accordance with those of a previous report which indicated the poor synergism of ZnO NPs with ampicillin against *P. aeruginosa* strain [104].

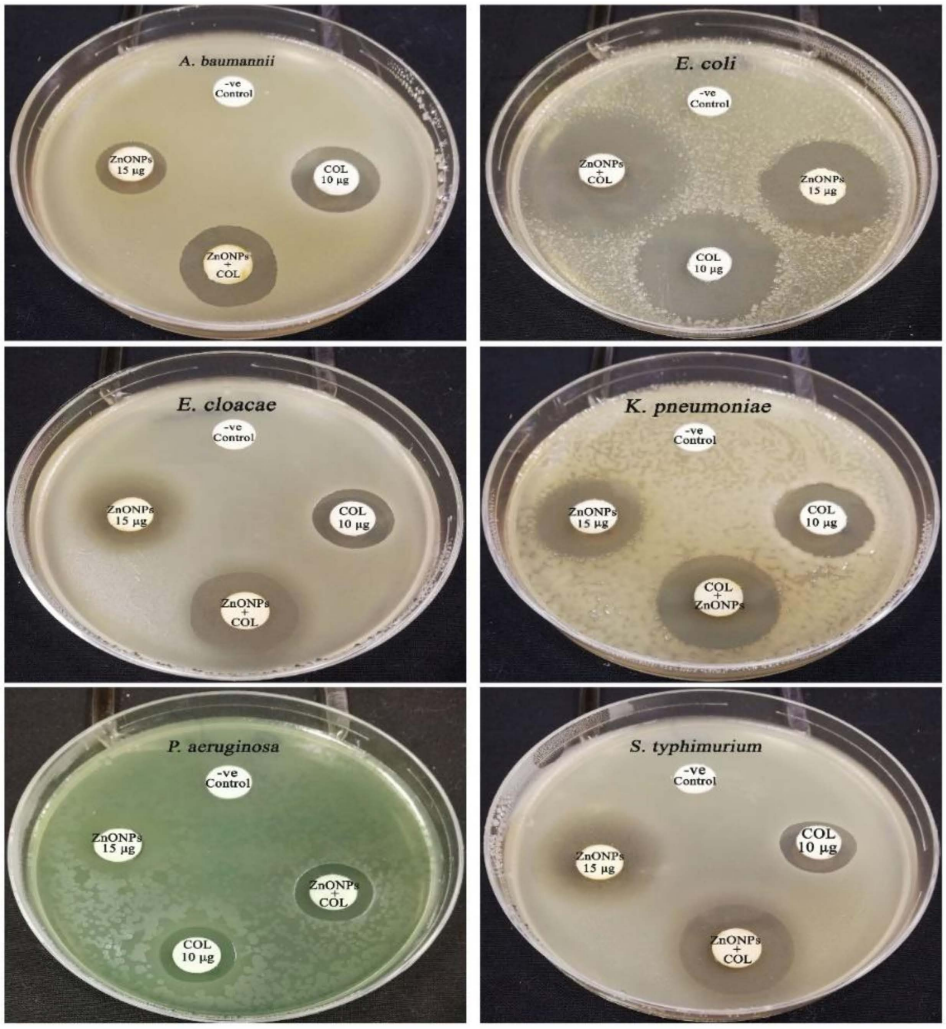

Figure 12. Synergistic patterns of the biogenic zinc oxide nanoparticles with colistin against the tested strains.

Moreover, the biosynthesized ZnO NPs exposed synergistic potency with colistin antibiotic against *K. pneumoniae*, *A. baumannii*, *S. typhimurium* and *E. cloacae* strains recording relative synergism percentages of 79.07, 75.04, 75.25 and 56.28%, respectively. The synergistic potency of the combined ZnO NPs and colistin antibiotic against *K. pneumoniae* was not significantly different compared to their efficiency against *A. baumannii* and *S. typhimurium* strains ($p > 0.05$) (Figure 13). In contrast, the synergistic potency of colistin with ZnO NPs against *E. coli* strain was significantly higher compared to the other strains ($p \leq 0.05$).

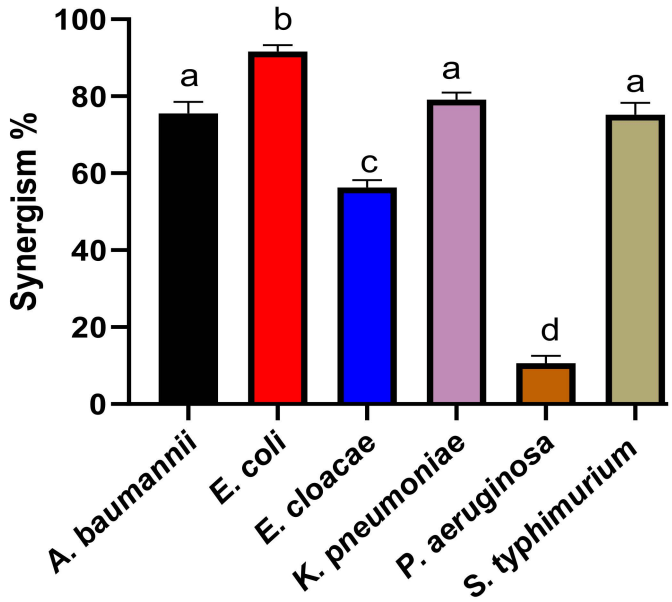

Figure 13. Synergistic antibacterial potency of the biosynthesized ZnO NPs with colistin against different bacterial strains. Different letters revealed that values were significantly different ($p \leq 0.05$).

When the combined antibacterial impact of ZnO NPs and antibiotic is greater than the effect of antibiotic alone, it is indicated that the synergistic potency of ZnO NPs + antibiotic combination (which could be accredited to that both of ZnO NPs and antibiotics) are targeting various cellular components [105]. Hence, we hypothesized that both the colistin antibiotic and the green ZnO NPs synthesized using water extract of *O. majorana* leaves targeted different cellular targets in order to reveal synergistic antibacterial activity. In this regard, the colistin antibiotic was reported to target the major structural component of gram-negative bacterial cells' outer membrane, which is known as lipopolysaccharide [106]. As a result, the colistin antibiotic's impact on lipopolysaccharides causes membrane breakdown, permitting the uptake of ZnO NPs that target the cellular components, leading to the induction of bacterial cell death [107]. The bioformulated ZnO NPs produce reactive oxygen species (ROS), such as hydrogen peroxide (H_2O_2), a potent oxidizing agent known to be toxic to bacterial cells [108]. The discharged ROS interacts with cellular components as DNA, protein, and lipids, leading to their disruption and induction of cell death [109]. In addition, ROS impairs the oxidative hemostasis of a cell, leading to the generation of oxidative stress and consequently causes bacterial cell death [110].

4. Conclusions

The present investigation proved the effectiveness of the green route for formulating ZnO NPs utilizing aqueous extract from *O. majorana* leaves. These nanomaterials demonstrated a potent antibacterial proficiency against the tested nosocomial bacterial pathogens. Accordingly, the high antibacterial potency of the biogenic ZnO NPs could be ascribed to the distinctive physicochemical features of these nanomaterials as the small nanosize of 12.467 nm. Additionally, the bioformulated ZnO nanomaterials revealed a potent synergistic effect with colistin against the concerned strains, indicating the potential use of ZnO NPs combined with colistin as effective antimicrobial agent against the nosocomial multidrug-resistant pathogens. Additionally, the combination of colistin and ZnO NPs may be a source for developing efficient coatings for usage in intensive care units, allowing for the efficient management of hospital-acquired infections.

Author Contributions: Conceptualization, M.T.Y. and A.A.A.-A.; methodology, M.T.Y.; software, M.T.Y.; validation, M.T.Y., A.A.A.-A. and F.O.A.-O.; formal analysis, M.T.Y., A.A.A.-A. and F.O.A.-O.; investigation, M.T.Y.; resources, A.A.A.-A.; data curation, M.T.Y. and K.M.; writing—original draft preparation, M.T.Y.; writing—review and editing, M.T.Y., A.A.A.-A. and F.O.A.-O.; visualization, M.T.Y., A.A.A.-A. and F.O.A.-O.; supervision, A.A.A.-A. and F.O.A.-O.; project administration, A.A.A.-A.; funding acquisition, F.O.A.-O. All authors have read and agreed to the published version of the manuscript.

Funding: This research project was supported by a grant from the Researchers Supporting Project number (RSP-2021/114), King Saud University, Riyadh, Saudi Arabia.

Data Availability Statement: The datasets used and/or analyzed during the current study are available from the corresponding author upon reasonable request.

Acknowledgments: The authors would like to extend their sincere appreciation to the Researchers Supporting Project number (RSP-2021/114), King Saud University, Riyadh, Saudi Arabia.

Conflicts of Interest: The authors declare no conflict of interest.

References

1. Gajdács, M.; Urbán, E.; Stájer, A.; Baráth, Z. Antimicrobial resistance in the context of the sustainable development goals: A brief review. *Eur. J. Investig. Health Psychol. Educ.* **2021**, *11*, 71–82. [CrossRef] [PubMed]
2. World Health Organization. Antimicrobial Resistance: Global Report on Surveillance 2014. 2014. Available online: https://www.who.int/publications/i/item/9789241564748 (accessed on 26 June 2019).
3. Terreni, M.; Taccani, M.; Pregnolato, M. New antibiotics for multidrug-resistant bacterial strains: Latest research developments and future perspectives. *Molecules* **2021**, *26*, 2671. [CrossRef] [PubMed]
4. Mulani, M.S.; Kamble, E.E.; Kumkar, S.N.; Tawre, M.S.; Pardesi, K.R. Emerging strategies to combat ESKAPE pathogens in the era of antimicrobial resistance: A review. *Front. Microbiol.* **2019**, *10*, 539. [CrossRef] [PubMed]
5. Djordjevic, Z.; Folic, M.M.; Zivic, Z.; Markovic, V.; Jankovic, S.M. Nosocomial urinary tract infections caused by *Pseudomonas aeruginosa* and *Acinetobacter* species: Sensitivity to antibiotics and risk factors. *Am. J. Infect. Control* **2013**, *41*, 1182–1187. [CrossRef]
6. Zhang, S.; Seeberger, P.H. Total Syntheses of Conjugation-Ready Repeating Units of *Acinetobacter baumannii* AB5075 for Glycoconjugate Vaccine Development. *Chem. Eur. J.* **2021**, *27*, 17444–17451. [CrossRef]
7. Lupo, A.; Haenni, M.; Madec, J.Y. Antimicrobial resistance in *Acinetobacter* spp. and *Pseudomonas* spp. *Microbiol. Spectr.* **2018**, *6*. [CrossRef]
8. Diggle, S.P.; Whiteley, M. Microbe Profile: *Pseudomonas aeruginosa*: Opportunistic pathogen and lab rat. *Microbiology* **2020**, *166*, 30. [CrossRef]
9. Pachori, P.; Gothalwal, R.; Gandhi, P. Emergence of antibiotic resistance *Pseudomonas aeruginosa* in intensive care unit; a critical review. *Genes Dis.* **2019**, *6*, 109–119. [CrossRef]
10. Mohd Asri, N.A.; Ahmad, S.; Mohamud, R.; Mohd Hanafi, N.; Mohd Zaidi, N.F.; Irekeola, A.A.; Shueb, R.H.; Yee, L.Y.; Noor, N.H.; Mustafa, F.H.; et al. Global prevalence of nosocomial multidrug-resistant *Klebsiella pneumoniae*: A systematic review and meta-analysis. *Antibiotics* **2021**, *10*, 1508. [CrossRef]
11. Lou, T.; Du, X.; Zhang, P.; Shi, Q.; Han, X.; Lan, P.; Yan, R.; Hu, H.; Wang, Y.; Wu, X.; et al. Risk factors for infection and mortality caused by carbapenem-resistant *Klebsiella pneumoniae*: A large multicentre case–control and cohort study. *J. Infect.* **2022**, *84*, 637–647. [CrossRef]
12. Davin-Regli, A.; Pagès, J.M. *Enterobacter aerogenes* and *Enterobacter cloacae*; versatile bacterial pathogens confronting antibiotic treatment. *Front. Microbiol.* **2015**, *6*, 392. [CrossRef] [PubMed]
13. Anju, V.T.; Siddhardha, B.; Dyavaiah, M. Enterobacter infections and antimicrobial drug resistance. In *Model Organisms for Microbial Pathogenesis, Biofilm Formation and Antimicrobial Drug Discovery*; Springer: Singapore, 2020; pp. 175–194.
14. Öztürk, R.; Murt, A. Epidemiology of urological infections: A global burden. *World J. Urol.* **2020**, *38*, 2669–2679. [CrossRef] [PubMed]
15. Australian Commission on Safety and Quality in Health Care. AURA 2019: Third Australian Report on Antimicrobial Use and Resistance in Human Health. 2019. Available online: https://www.safetyandquality.gov.au/sites/default/files/2019-06/AURA-2019-Report.pdf (accessed on 10 November 2019).
16. Chlebicz, A.; Śliżewska, K. Campylobacteriosis, salmonellosis, yersiniosis, and listeriosis as zoonotic foodborne diseases: A review. *Int. J. Environ. Health Res.* **2018**, *15*, 863. [CrossRef] [PubMed]
17. Jajere, S.M. A review of *Salmonella enterica* with particular focus on the pathogenicity and virulence factors, host specificity and antimicrobial resistance including multidrug resistance. *Vet. World* **2019**, *12*, 504. [CrossRef]
18. Ahmed, H.M.; Roy, A.; Wahab, M.; Ahmed, M.; Othman-Qadir, G.; Elesawy, B.H.; Khandaker, M.U.; Islam, M.N.; Emran, T.B. Applications of nanomaterials in agrifood and pharmaceutical industry. *J. Nanomater.* **2021**, *2021*, 1472096. [CrossRef]
19. Dutta, G.; Sugumaran, A. Bioengineered zinc oxide nanoparticles: Chemical, green, biological fabrication methods and its potential biomedical applications. *J. Drug Deliv. Sci. Technol.* **2021**, *66*, 102853. [CrossRef]

20. Nikolova, M.P.; Chavali, M.S. Metal oxide nanoparticles as biomedical materials. *Biomimetics* **2020**, *5*, 27. [CrossRef]
21. Salem, S.S.; Fouda, A. Green synthesis of metallic nanoparticles and their prospective biotechnological applications: An overview. *Biol. Trace Elem. Res.* **2021**, *199*, 344–370. [CrossRef]
22. Ahmad, W.; Kalra, D. Green synthesis, characterization and anti microbial activities of ZnO nanoparticles using Euphorbia hirta leaf extract. *J. King Saud Univ. Sci.* **2020**, *32*, 2358–2364. [CrossRef]
23. Yazdanian, M.; Rostamzadeh, P.; Rahbar, M.; Alam, M.; Abbasi, K.; Tahmasebi, E.; Tebyaniyan, H.; Ranjbar, R.; Seifalian, A.; Yazdanian, A. The Potential Application of Green-Synthesized Metal Nanoparticles in Dentistry: A Comprehensive Review. *Bioinorg. Chem. Appl.* **2022**, *2022*, 2311910. [CrossRef]
24. Remya, V.R.; Abitha, V.K.; Rajput, P.S.; Rane, A.V.; Dutta, A. Silver nanoparticles green synthesis: A mini review. *Chem. Int.* **2017**, *3*, 165–171.
25. Salunke, B.K.; Sathiyamoorthi, E.; Tran, T.K.; Kim, B.S. Phyto-synthesized silver nanoparticles for biological applications. *Korean J. Chem. Eng.* **2017**, *34*, 943–951. [CrossRef]
26. El Shafey, A.M. Green synthesis of metal and metal oxide nanoparticles from plant leaf extracts and their applications: A review. *Green Process. Synth.* **2020**, *9*, 304–339. [CrossRef]
27. Vijayaraghavan, K.; Ashokkumar, T. Plant-mediated biosynthesis of metallic nanoparticles: A review of literature, factors affecting synthesis, characterization techniques and applications. *J. Environ. Chem. Eng.* **2017**, *5*, 4866–4883. [CrossRef]
28. Alrajhi, A.H.; Ahmed, N.M.; Al Shafouri, M.; Almessiere, M.A. Green synthesis of zinc oxide nanoparticles using salvia officials extract. *Mater. Sci. Semicond. Process.* **2021**, *125*, 105641. [CrossRef]
29. Fagier, M.A. Plant-mediated biosynthesis and photocatalysis activities of zinc oxide nanoparticles: A prospect towards dyes mineralization. *J. Nanotechnol.* **2021**, *2021*, 6629180. [CrossRef]
30. Smijs, T.G.; Pavel, S. Titanium dioxide and zinc oxide nanoparticles in sunscreens: Focus on their safety and effectiveness. *Nanotechnol. Sci. Appl.* **2011**, *4*, 95. [CrossRef] [PubMed]
31. Anjum, S.; Hashim, M.; Malik, S.A.; Khan, M.; Lorenzo, J.M.; Abbasi, B.H.; Hano, C. Recent advances in zinc oxide nanoparticles (Zno nps) for cancer diagnosis, target drug delivery, and treatment. *Cancers* **2021**, *13*, 4570. [CrossRef]
32. Aldeen, T.S.; Mohamed, H.E.A.; Maaza, M. ZnO nanoparticles prepared via a green synthesis approach: Physical properties, photocatalytic and antibacterial activity. *J. Phys. Chem. Solids* **2022**, *160*, 110313. [CrossRef]
33. Archana, P.; Janarthanan, B.; Bhuvana, S.; Rajiv, P.; Sharmila, S. Concert of zinc oxide nanoparticles synthesized using *Cucumis melo* by green synthesis and the antibacterial activity on pathogenic bacteria. *Inorg. Chem. Commun.* **2022**, *137*, 109255.
34. Azimpanah, R.; Solati, Z.; Hashemi, M. Synthesis of ZnO nanoparticles with Antibacterial properties using terminalia catappa leaf extract. *Chem. Eng. Technol.* **2022**, *45*, 658–666. [CrossRef]
35. Alshameri, A.W.; Owais, M. Antibacterial and cytotoxic potency of the plant-mediated synthesis of metallic nanoparticles Ag NPs and ZnO NPs: A Review. *OpenNano* **2022**, *8*, 100077. [CrossRef]
36. Namasivayam, S.K.R.; Prasanna, M.; Subathra, S. Synergistic antibacterial activity of zinc oxide nanoparticles with antibiotics against the human pathogenic bacteria. *J. Chem. Pharm. Res.* **2015**, *7*, 133–138.
37. Farzana, R.; Iqra, P.; Shafaq, F.; Sumaira, S.; Zakia, K.; Hunaiza, T.; Husna, M. Antimicrobial behavior of zinc oxide nanoparticles and β-lactam antibiotics against pathogenic Bacteria. *Arch. Clin. Microbiol.* **2017**, *8*, 57.
38. Paudel, P.N.; Satyal, P.; Satyal, R.; Setzer, W.N.; Gyawali, R. Chemical Composition, Enantiomeric Distribution, Antimicrobial and Antioxidant Activities of Origanum majorana L. Essential Oil from Nepal. *Molecules* **2022**, *27*, 6136. [CrossRef] [PubMed]
39. Bouyahya, A.; Chamkhi, I.; Benali, T.; Guaouguaou, F.E.; Balahbib, A.; El Omari, N.; Taha, D.; Belmehdi, O.; Ghokhan, Z.; El Menyiy, N. Traditional use, phytochemistry, toxicology, and pharmacology of *Origanum majorana* L. *J. Ethnopharmacol.* **2021**, *265*, 113318. [CrossRef] [PubMed]
40. Fadwa, A.O.; Alkoblan, D.K.; Mateen, A.; Albarag, A.M. Synergistic effects of zinc oxide nanoparticles and various antibiotics combination against *Pseudomonas aeruginosa* clinically isolated bacterial strains. *Saudi J. Biol. Sci.* **2021**, *28*, 928–935. [CrossRef]
41. Yassin, M.T.; Mostafa, A.A.F.; Al-Askar, A.A.; Al-Otibi, F.O. Synergistic antibacterial activity of green synthesized silver nanomaterials with colistin antibiotic against multidrug-resistant bacterial pathogens. *Crystals* **2022**, *12*, 1057. [CrossRef]
42. Lopez-Carrizales, M.; Pérez-Díaz, M.A.; Mendoza-Mendoza, E.; Peralta-Rodríguez, R.D.; Ojeda-Galván, H.J.; Portales-Pérez, D.; Magaña-Aquino, M.; Sánchez-Sánchez, R.; Martinez-Gutierrez, F. Green, novel, and one-step synthesis of silver oxide nanoparticles: Antimicrobial activity, synergism with antibiotics, and cytotoxic studies. *New J. Chem.* **2022**, *46*, 17841–17853. [CrossRef]
43. Yassin, M.T.; Mostafa, A.A.F.; Al-Askar, A.A.; Al-Otibi, F.O. Synergistic Antifungal Efficiency of Biogenic Silver Nanoparticles with Itraconazole against Multidrug-Resistant Candidal Strains. *Crystals* **2022**, *12*, 816. [CrossRef]
44. Yassin, M.T.; Mostafa, A.A.F.; Al-Askar, A.A.; Sayed, S.R. In vitro antimicrobial activity of Thymus vulgaris extracts against some nosocomial and food poisoning bacterial strains. *Process. Biochem* **2022**, *115*, 152–159. [CrossRef]
45. Yassin, M.T.; Mostafa, A.A.F.; Al-Askar, A.A. In vitro anticandidal potency of Syzygium aromaticum (clove) extracts against vaginal candidiasis. *BMC Complement. Altern. Med.* **2020**, *20*, 25. [CrossRef] [PubMed]
46. Yassin, M.T.; Mostafa, A.A.; Al-Askar, A.A. Anticandidal and anti-carcinogenic activities of Mentha longifolia (Wild Mint) extracts in vitro. *J. King Saud Univ. Sci.* **2020**, *32*, 2046–2052. [CrossRef]
47. Yassin, M.T.; Mostafa, A.A.F.; Al-Askar, A.A.; Alkhelaif, A.S. In vitro antimicrobial potency of Elettaria cardamomum ethanolic extract against multidrug resistant of food poisoning bacterial strains. *J. King Saud Univ. Sci.* **2022**, *34*, 102167. [CrossRef]

48. Yassin, M.T.; Mostafa, A.A.F.; Al-Askar, A.A.; Al-Otibi, F.O. Facile Green Synthesis of Zinc Oxide Nanoparticles with Potential Synergistic Activity with Common Antifungal Agents against Multidrug-Resistant Candidal Strains. *Crystals* **2022**, *12*, 774. [CrossRef]
49. Tang, Q.; Xia, H.; Liang, W.; Huo, X.; Wei, X. Synthesis and characterization of zinc oxide nanoparticles from Morus nigra and its anticancer activity of AGS gastric cancer cells. *J. Photochem. Photobiol. B Biol.* **2020**, *202*, 111698. [CrossRef]
50. Clinical and Laboratory Standards. *Performance Standards for Antimicrobial Disk Susceptibility Tests*; Approved Standard M2-A8; Clinical and Laboratory Standards Institute (CLSI): Wayne, PA, USA, 2003.
51. Yassin, M.T.; Mostafa, A.A.F.; Al Askar, A.A. In Vitro Evaluation of Biological Activities and Phytochemical Analysis of Different Solvent Extracts of *Punica granatum* L. (Pomegranate) Peels. *Plants* **2021**, *10*, 2742. [CrossRef]
52. Punjabi, K.; Mehta, S.; Chavan, R.; Chitalia, V.; Deogharkar, D.; Deshpande, S. Efficiency of biosynthesized silver and zinc nanoparticles against multi-drug resistant pathogens. *Front. Microbiol.* **2018**, *9*, 2207. [CrossRef]
53. Huang, W.; Yan, M.; Duan, H.; Bi, Y.; Cheng, X.; Yu, H. Synergistic antifungal activity of green synthesized silver nanoparticles and epoxiconazole against *Setosphaeria turcica*. *J. Nanomater.* **2020**, *2020*, 9535432. [CrossRef]
54. Lo, W.H.; Deng, F.S.; Chang, C.J.; Lin, C.H. Synergistic antifungal activity of chitosan with fluconazole against Candida albicans, Candida tropicalis, and fluconazole-resistant strains. *Molecules* **2020**, *25*, 5114. [CrossRef]
55. Moteriya, P.; Padalia, H.; Chanda, S. Characterization, synergistic antibacterial and free radical scavenging efficacy of silver nanoparticles synthesized using Cassia roxburghii leaf extract. *J. Genet. Eng. Biotechnol.* **2017**, *15*, 505–513. [CrossRef] [PubMed]
56. Sutradhar, P.; Saha, M. Green synthesis of zinc oxide nanoparticles using tomato (*Lycopersicon esculentum*) extract and its photovoltaic application. *J. Exp. Nanosci.* **2016**, *11*, 314–327. [CrossRef]
57. Parthasarathy, G.; Saroja, M.; Venkatachalam, M.; Evanjelene, V.K. Biological synthesis of zinc oxide nanoparticles from leaf extract of Curcuma neilgherrensis Wight. *Int. J. Mater. Sci.* **2017**, *12*, 73–86.
58. Valduga, A.T.; Gonçalves, I.L.; Magri, E.; Finzer, J.R.D. Chemistry, pharmacology and new trends in traditional functional and medicinal beverages. *Food Res. Int.* **2019**, *120*, 478–503. [CrossRef] [PubMed]
59. Flora, S.J. Structural, chemical and biological aspects of antioxidants for strategies against metal and metalloid exposure. *Oxid. Med. Cell. Longev.* **2009**, *2*, 191–206. [CrossRef] [PubMed]
60. Erenler, R.; Sen, O.; Aksit, H.; Demirtas, I.; Yaglioglu, A.S.; Elmastas, M.; Telci, I. Isolation and identification of chemical constituents from *Origanum majorana* and investigation of antiproliferative and antioxidant activities. *J. Sci. Food Agric.* **2016**, *96*, 822–836. [CrossRef]
61. Ahmed, S.; Chaudhry, S.A.; Ikram, S. A review on biogenic synthesis of ZnO nanoparticles using plant extracts and microbes: A prospect towards green chemistry. *J. Photochem. Photobiol. B Biol.* **2017**, *166*, 272–284. [CrossRef]
62. Yassin, M.T.; Mostafa, A.A.F.; Al-Askar, A.A.; Al-Otibi, F.O. Facile green synthesis of silver nanoparticles using aqueous leaf extract of *Origanum majorana* with potential bioactivity against multidrug resistant bacterial strains. *Crystals* **2022**, *12*, 603. [CrossRef]
63. Mohammadian, M.; Es'haghi, Z.; Hooshmand, S. Green and chemical synthesis of zinc oxide nanoparticles and size evaluation by UV–vis spectroscopy. *J. Nanomed. Res.* **2018**, *7*, 00175.
64. Babu, K.S.; Reddy, A.R.; Sujatha, C.; Reddy, K.V. Optimization of UV emission intensity of ZnO nanoparticles by changing the excitation wavelength. *Mater. Lett.* **2013**, *99*, 97–100. [CrossRef]
65. Fuku, X.; Diallo, A.; Maaza, M. Nanoscaled electrocatalytic optically modulated ZnO nanoparticles through green process of *Punica granatum* L. and their antibacterial activities. *Int. J. Electrochem. Sci.* **2016**, *2016*, 4682967.
66. Siva, N.; Sakthi, D.; Ragupathy, S.; Arun, V.; Kannadasan, N. Synthesis, structural, optical and photocatalytic behavior of Sn doped ZnO nanoparticles. *Mater. Sci. Eng. B* **2020**, *253*, 114497. [CrossRef]
67. Fatimah, I.; Pradita, R.Y.; Nurfalinda, A. Plant extract mediated of ZnO nanoparticles by using ethanol extract of *Mimosa pudica* leaves and coffee powder. *Procedia Eng.* **2016**, *148*, 43–48. [CrossRef]
68. Ngoepe, N.M.; Mbita, Z.; Mathipa, M.; Mketo, N.; Ntsendwana, B.; Hintsho-Mbita, N.C. Biogenic synthesis of ZnO nanoparticles using Monsonia burkeana for use in photocatalytic, antibacterial and anticancer applications. *Ceram. Int.* **2018**, *44*, 16999–17006. [CrossRef]
69. Falih, A.; Ahmed, N.M.; Rashid, M. Green synthesis of zinc oxide nanoparticles by fresh and dry alhagi plant. *Mater. Today Proc.* **2022**, *49*, 3624–3629. [CrossRef]
70. Khalil, A.T.; Ovais, M.; Ullah, I.; Ali, M.; Shinwari, Z.K.; Khamlich, S.; Maaza, M. *Sageretia thea* (Osbeck.) mediated synthesis of zinc oxide nanoparticles and its biological applications. *Nanomedicine* **2017**, *12*, 1767–1789. [CrossRef]
71. El-Belely, E.F.; Farag, M.M.; Said, H.A.; Amin, A.S.; Azab, E.; Gobouri, A.A.; Fouda, A. Green synthesis of zinc oxide nanoparticles (ZnO-NPs) using *Arthrospira platensis* (Class: Cyanophyceae) and evaluation of their biomedical activities. *Nanomaterials* **2021**, *11*, 95. [CrossRef]
72. Sultana, K.A.; Islam, M.T.; Silva, J.A.; Turley, R.S.; Hernandez-Viezcas, J.A.; Gardea-Torresdey, J.L.; Noveron, J.C. Sustainable synthesis of zinc oxide nanoparticles for photocatalytic degradation of organic pollutant and generation of hydroxyl radical. *J. Mol. Liq.* **2020**, *307*, 112931. [CrossRef]
73. Vimala, K.; Sundarraj, S.; Paulpandi, M.; Vengatesan, S.; Kannan, S. Green synthesized doxorubicin loaded zinc oxide nanoparticles regulates the Bax and Bcl-2 expression in breast and colon carcinoma. *Process. Biochem.* **2014**, *49*, 160–172. [CrossRef]

74. El-Hawwary, S.S.; Abd Almaksoud, H.M.; Saber, F.R.; Elimam, H.; Sayed, A.M.; El Raey, M.A.; Abdelmohsen, U.R. Green-synthesized zinc oxide nanoparticles, anti-Alzheimer potential and the metabolic profiling of Sabal blackburniana grown in Egypt supported by molecular modelling. *RSC Adv.* **2021**, *11*, 18009–18025. [CrossRef]
75. Gharagozlou, M.; Naghibi, S. Sensitization of ZnO nanoparticle by vitamin B12: Investigation of microstructure, FTIR and optical properties. *Mater. Res. Bull.* **2016**, *84*, 71–78. [CrossRef]
76. Acharya, T.R.; Lamichhane, P.; Wahab, R.; Chaudhary, D.K.; Shrestha, B.; Joshi, L.P.; Kaushik, N.K.; Choi, E.H. Study on the Synthesis of ZnO Nanoparticles Using *Azadirachta indica* Extracts for the Fabrication of a Gas Sensor. *Molecules* **2021**, *26*, 7685. [CrossRef]
77. Ghaffari, S.B.; Sarrafzadeh, M.H.; Fakhroueian, Z.; Shahriari, S.; Khorramizadeh, M.R. Functionalization of ZnO nanoparticles by 3-mercaptopropionic acid for aqueous curcumin delivery: Synthesis, characterization, and anticancer assessment. *Mater. Sci. Eng. C* **2017**, *79*, 465–472. [CrossRef] [PubMed]
78. Abdulmalek, S.; Eldala, A.; Awad, D.; Balbaa, M. Ameliorative effect of curcumin and zinc oxide nanoparticles on multiple mechanisms in obese rats with induced type 2 diabetes. *Sci. Rep* **2021**, *11*, 20677. [CrossRef] [PubMed]
79. Singh, A.; Kaushik, M. Physicochemical investigations of zinc oxide nanoparticles synthesized from *Azadirachta Indica* (Neem) leaf extract and their interaction with Calf-Thymus DNA. *Results Phys.* **2019**, *13*, 102168. [CrossRef]
80. Bhuyan, T.; Mishra, K.; Khanuja, M.; Prasad, R.; Varma, A. Biosynthesis of zinc oxide nanoparticles from Azadirachta indica for antibacterial and photocatalytic applications. *Mater. Sci. Semicond. Process* **2015**, *32*, 55–61. [CrossRef]
81. Khan, M.S.; Dhavan, P.P.; Jadhav, B.L.; Shimpi, N.G. Ultrasound-Assisted Green Synthesis of Ag-Decorated ZnO Nanoparticles Using *Excoecaria agallocha* Leaf Extract and Evaluation of Their Photocatalytic and Biological Activity. *Chem. Sel.* **2020**, *5*, 12660–12671.
82. Abdelmigid, H.M.; Hussien, N.A.; Alyamani, A.A.; Morsi, M.M.; AlSufyani, N.M.; Kadi, H.A. Green Synthesis of Zinc Oxide Nanoparticles Using Pomegranate Fruit Peel and Solid Coffee Grounds vs. Chemical Method of Synthesis, with Their Biocompatibility and Antibacterial Properties Investigation. *Molecules* **2022**, *27*, 1236. [CrossRef]
83. Ifeanyichukwu, U.L.; Fayemi, O.E.; Ateba, C.N. Green synthesis of zinc oxide nanoparticles from pomegranate (*Punica granatum*) extracts and characterization of their antibacterial activity. *Molecules* **2020**, *25*, 4521. [CrossRef]
84. Vijayakumar, S.; Divya, M.; Vaseeharan, B.; Ranjan, S.; Kalaiselvi, V.; Dasgupta, N.; Chen, J.; Durán-Lara, E.F. Biogenic preparation and characterization of ZnO nanoparticles from natural polysaccharide *Azadirachta indica*. L. (neem gum) and its clinical implications. *J. Clust. Sci.* **2021**, *32*, 983–993. [CrossRef]
85. Gawade, V.V.; Gavade, N.L.; Shinde, H.M.; Babar, S.B.; Kadam, A.N.; Garadkar, K.M. Green synthesis of ZnO nanoparticles by using *Calotropis procera* leaves for the photodegradation of methyl orange. *J. Mater. Sci. Mater. Electron.* **2017**, *28*, 14033–14039. [CrossRef]
86. Vijayakumar, S.; Vinoj, G.; Malaikozhundan, B.; Shanthi, S.; Vaseeharan, B. *Plectranthus amboinicus* leaf extract mediated synthesis of zinc oxide nanoparticles and its control of methicillin resistant Staphylococcus aureus biofilm and blood sucking mosquito larvae. *Spectrochim. Acta A Mol. Biomol. Spectrosc.* **2015**, *137*, 886–891. [CrossRef] [PubMed]
87. Radwan, A.M.; Aboelfetoh, E.F.; Kimura, T.; Mohamed, T.M.; El-Keiy, M.M. Fenugreek-mediated synthesis of zinc oxide nanoparticles and evaluation of its in vitro and in vivo antitumor potency. *Biomed. Res. Ther.* **2021**, *8*, 4483–4496. [CrossRef]
88. Consolo, V.F.; Torres-Nicolini, A.; Alvarez, V.A. Mycosinthetized Ag, CuO and ZnO nanoparticles from a promising *Trichoderma harzianum* strain and their antifungal potential against important phytopathogens. *Sci. Rep.* **2020**, *10*, 20499. [CrossRef]
89. Kaur, T.; Bala, M.; Kumar, G.; Vyas, A. Biosynthesis of zinc oxide nanoparticles via endophyte Trichoderma viride and evaluation of their antimicrobial and antioxidant properties. *Arch. Microbiol.* **2022**, *204*, 620. [CrossRef]
90. Elamawi, R.M.; Al-Harbi, R.E.; Hendi, A.A. Biosynthesis and characterization of silver nanoparticles using *Trichoderma longibrachiatum* and their effect on phytopathogenic fungi. *Egypt. J. Biol. Pest Control* **2018**, *28*, 28. [CrossRef]
91. Al Sharie, A.H.; El-Elimat, T.; Darweesh, R.S.; Swedan, S.; Shubair, Z.; Al-Qiam, R.; Albarqi, H. Green synthesis of zinc oxide nanoflowers using Hypericum triquetrifolium extract: Characterization, antibacterial activity and cytotoxicity against lung cancer A549 cells. *Appl. Organomet. Chem.* **2020**, *34*, e5667. [CrossRef]
92. Alahmad, A.; Feldhoff, A.; Bigall, N.C.; Rusch, P.; Scheper, T.; Walter, J.G. *Hypericum perforatum* L.-mediated green synthesis of silver nanoparticles exhibiting antioxidant and anticancer activities. *Nanomaterials* **2021**, *11*, 487. [CrossRef]
93. Ramanarayanan, R.; Bhabhina, N.M.; Dharsana, M.V.; Nivedita, C.V.; Sindhu, S. Green synthesis of zinc oxide nanoparticles using extract of *Averrhoa bilimbi* (L) and their photoelectrode applications. *Mater. Today Proc.* **2018**, *5*, 16472–16477. [CrossRef]
94. Iqbal, J.; Abbasi, B.A.; Mahmood, T.; Hameed, S.; Munir, A.; Kanwal, S. Green synthesis and characterizations of Nickel oxide nanoparticles using leaf extract of *Rhamnus virgata* and their potential biological applications. *Appl. Organomet. Chem.* **2019**, *33*, e4950. [CrossRef]
95. Abdelbaky, A.S.; El-Mageed, A.; Taia, A.; Babalghith, A.O.; Selim, S.; Mohamed, A.M. Green Synthesis and Characterization of ZnO Nanoparticles Using *Pelargonium odoratissimum* (L.) Aqueous Leaf Extract and Their Antioxidant, Antibacterial and Anti-inflammatory Activities. *Antioxidants* **2022**, *11*, 1444. [CrossRef] [PubMed]
96. Velsankar, K.; Sudhahar, S.; Maheshwaran, G. Effect of biosynthesis of ZnO nanoparticles via Cucurbita seed extract on Culex tritaeniorhynchus mosquito larvae with its biological applications. *J. Photochem. Photobiol. B Biol.* **2019**, *200*, 111650.
97. Subramanian, H.; Krishnan, M.; Mahalingam, A. Photocatalytic dye degradation and photoexcited anti-microbial activities of green zinc oxide nanoparticles synthesized via *Sargassum muticum* extracts. *RSC Adv.* **2022**, *12*, 985–997. [CrossRef] [PubMed]

98. Rahman, A.; Harunsani, M.H.; Tan, A.L.; Khan, M.M. Zinc oxide and zinc oxide-based nanostructures: Biogenic and phytogenic synthesis, properties and applications. *Bioprocess Biosyst. Eng.* **2021**, *44*, 1333–1372. [CrossRef]
99. Okeke, I.S.; Agwu, K.K.; Ubachukwu, A.A.; Madiba, I.G.; Maaza, M.; Whyte, G.M.; Ezema, F.I. Impact of particle size and surface defects on antibacterial and photocatalytic activities of undoped and Mg-doped ZnO nanoparticles, biosynthesized using one-step simple process. *Vacuum* **2020**, *187*, 110110. [CrossRef]
100. Onyszko, M.; Zywicka, A.; Wenelska, K.; Mijowska, E. Revealing the Influence of the Shape, Size, and Aspect Ratio of ZnO Nanoparticles on Antibacterial and Mechanical Performance of Cellulose Fibers Based Paper. *Part. Part. Syst. Charact* **2022**, *39*, 2200014. [CrossRef]
101. Zhu, X.; Wang, J.; Cai, L.; Wu, Y.; Ji, M.; Jiang, H.; Chen, J. Dissection of the antibacterial mechanism of zinc oxide nanoparticles with manipulable nanoscale morphologies. *J. Hazard. Mater.* **2022**, *430*, 128436. [CrossRef]
102. De Oliveira, D.M.; Forde, B.M.; Kidd, T.J.; Harris, P.N.; Schembri, M.A.; Beatson, S.A.; Paterson, D.L.; Walker, M.J. Antimicrobial resistance in ESKAPE pathogens. *Clin. Microbiol. Rev.* **2020**, *33*, e00181-19. [CrossRef]
103. Abo-Shama, U.H.; el-Gendy, H.; Mousa, W.S.; Hamouda, R.A.; Yousuf, W.E.; Hetta, H.F.; Abdeen, E.E. Synergistic and antagonistic effects of metal nanoparticles in combination with antibiotics against some reference strains of pathogenic microorganisms. *Infect. Drug Resist.* **2020**, *13*, 351–362. [CrossRef]
104. Reyes-Torres, M.A.; Mendoza-Mendoza, E.; Miranda-Hernández, Á.M.; Pérez-Díaz, M.A.; López-Carrizales, M.; Peralta-Rodríguez, R.D.; Martinez-Gutierrez, F. Synthesis of CuO and ZnO nanoparticles by a novel green route: Antimicrobial activity, cytotoxic effects and their synergism with ampicillin. *Ceram. Int.* **2019**, *45*, 24461–24468. [CrossRef]
105. Ribeiro, A.I.; Dias, A.M.; Zille, A. Synergistic effects between metal nanoparticles and commercial antimicrobial agents: A Review. *ACS Appl. Nano Mater.* **2022**, *5*, 3030–3064. [CrossRef]
106. Ebbensgaard, A.; Mordhorst, H.; Aarestrup, F.M.; Hansen, E.B. The role of outer membrane proteins and lipopolysaccharides for the sensitivity of Escherichia coli to antimicrobial peptides. *Front. Microbiol.* **2018**, *9*, 2153. [CrossRef]
107. Ledger, E.V.; Sabnis, A.; Edwards, A.M. Polymyxin and lipopeptide antibiotics: Membrane-targeting drugs of last resort. *Microbiology* **2022**, *168*, 001136. [CrossRef]
108. Ahmadi Shadmehri, A.; Namvar, F. A Review on Green Synthesis, Cytotoxicity Mechanism and Antibacterial Activity of Zno-NPs. *J. Res. Appl. Basic Med. Res.* **2020**, *6*, 23–31.
109. Singh, A.; Singh, N.Á.; Afzal, S.; Singh, T.; Hussain, I. Zinc oxide nanoparticles: A review of their biological synthesis, antimicrobial activity, uptake, translocation and biotransformation in plants. *J. Mater. Sci.* **2018**, *53*, 185–201. [CrossRef]
110. Siddiqi, K.S.; Husen, A. Properties of zinc oxide nanoparticles and their activity against microbes. *Nanoscale Res. Lett.* **2018**, *13*, 141. [CrossRef]